Ultraviolet Spectropolarimetry: Conservative and Nonconservative Mass Transfer in OB Interacting Binaries

Geraldine J. Peters[1], Kenneth G. Gayley[2], Richard Ignace[3], Carol E. Jones[4], Yaël Nazé[5], Nicole St-Louis[6], Heloise Stevance[7], Jorick S .Vink[8], Noel D. Richardson[9], Jennifer L. Hoffman[10], Jamie R. Lomax[11], Tomer Shenar[12], Andrew G .Fullard[13] and Paul A. Scowen[14]

*Corresponding author(s). E-mail(s): gpeters@usc.edu;

Abstract

The current consensus is that at least half of the OB stars are formed in binary or multiple star systems. The evolution of OB stars is greatly influenced by whether the stars begin as close binaries, and the evolution of the binary systems depend on whether the mass transfer is conservative or nonconservative. FUV/NUV spectropolarimetry is poised to answer the latter question. This paper discusses how the *Polstar* spectropolarimetry mission can characterize the degree of nonconservative mass transfer that occurs at various stages of binary evolution, from the initial mass reversal to the late Algol phase, and quantify its amount. The proposed instrument combines spectroscopic and polarimetric capabilities, where the spectroscopy can resolve Doppler shifts in UV resonance lines with 10 km/s precision, and polarimetry can resolve linear polarization with $\mathbf{10^{-3}}$ precision or better. The spectroscopy will identify absorption by mass streams and other plasmas seen in projection against the stellar disk as a function of orbital phase, as well as scattering from extended splash structures, including jets. The polarimetry tracks the light coming from material not seen against the stellar disk, allowing the geometry of the scattering to be tracked, resolving ambiguities left by the spectroscopy and light-curve information. For example, nonconservative mass streams ejected in the polar direction will produce polarization of the opposite sign from conservative transfer accreting in the orbital plane. Time domain coverage over a range of phases of the binary orbit are well supported by the *Polstar* observing strategy. Special attention will be given to the epochs of enhanced systemic mass loss that have been identified from *IUE* observations (pre-mass reversal and tangential gas stream impact). We show how the history of systemic mass and angular momentum loss/gain episodes can be inferred via ensemble evolution through the r–q diagram. Combining the above elements will significantly improve our understanding of the mass transfer process and the amount of mass that can escape from the system, an important channel for changing the final mass and ultimate supernova of a large number of massive stars found in binaries at close enough separation to undergo interaction.

Keywords: Algol variable stars(24); Be stars (142); Close binary stars (254); Circumstellar matter(241); Early-type emission stars (428); Instruments: ; Multiple star evolution (2153); NASA: MIDEX; O subdwarf stars (1138); Spectropolarimetry (1973); Stellar mass loss (1613); Ultraviolet astronomy (1736)

1 Introduction

Most massive stars are born in multiple systems. Spectroscopic surveys of the Tarantula Nebula and Galaxy suggest that between half and two thirds of massive stars undergo binary interactions at some point in their lifetimes (Sana et al, 2012, 2013). Mass transfer is an important step in the evolution of most massive binary systems: it alters the stellar masses, resulting in stripped stars and rejuvenation, which affects the lifetime and death of the stars. As has been called out in the Astro2020 decadal survey, binary interactions are crucial to understand stellar evolution, including the creation of stripped envelope supernovae and kilonovae (Paczyński, 1971; Langer, 2012; Eldridge et al, 2013; Yoon, 2015; Tauris et al, 2017; Laplace et al, 2021), which are key contributors to the chemical evolution of the ISM and provide an important source of feedback. Also, mass lost by a star is not necessarily all accreted by its companion, and escaping mass streams can reduce the final masses of stars by a significant amount that has not been well quantified either observationally or theoretically. In this paper we discuss how the *Polstar* spectropolarimetry mission (Scowen et al, 2022) is poised to characterize the degree of nonconservative mass transfer that occurs during close binary evolution, from the initial mass reversal to the late Algol stage, and quantify its amount.

Given the high ionization of massive-star winds, jets, and other circumstellar structures, Thomson scattering (electron scattering) is expected to dominate the induced polarization, producing a useful sensitivity to the geometry of scattering regions that can be used to resolve ambiguities in the spectroscopic observations. The classic pioneering model by Brown et al (1978, BME hereafter) approximates the time-varying continuum polarization caused by the illumination of stellar winds in a binary system viewed at an arbitrary inclination angle. In this model, the scattering region is described as an optically thin electron gas. The envelope pattern is assumed to co-rotate with the illumination sources, appropriate for steady-state systems in circular orbit. The illuminators consist of one point source at the center of the scattering region and an additional external point source representing the companion.

Brown et al (1982) extended the BME model to consider elliptical orbits, and Fox (1994) further extended the formalism to consider finite illuminators. Fox (1994) showed that occultation is only important in very close binary systems, where separation is less than 10 times the radius of the primary star. However, none of these enhancements to the theory included mass streams involved in non-conservative mass transfer. Furthermore, the time and wavelength dependence of the polarization from escaping mass, which could provide unique constraints and help separate the intrinsic polarization from interstellar polarization (ISP), has not been modeled. However, hints of such polarized signals associated with non-conservative mass transfer have been observed in several systems (e.g.β Lyr, Hoffman et al, 1998; Lomax et al, 2012a) and extending these observations into the UV, the domain of strongest stellar irradiation for hot stars, will help quantify the degree of mass loss.

The optically-thin polarization models are crucial since they provide basic insights into information that continuum polarization can provide. In the case of an axisymetric envelope around a point source, the observed polarization only depends on three parameters: the optical depth τ of the envelope, the shape of the envelope (described by a single parameter γ defined below), and the inclination i of the symmetry axis relative to the observer. If the envelope is oblate, the observed polarization is parallel to the symmetry axis. Conversely, the observed polarization is perpendicular to the symmetry axis for a prolate envelope. These results are easily understood: for a prolate envelope the density is highest along the poles, and it is these regions –for which the electric vector and hence polarization is perpendicular to the symmetry axis– that will contribute most to the observed flux. This is one of the ways *Polstar's* polarimetric capability can supplement spectroscopic information, helping to describe the mass-transfer structure.

In optically thick envelopes, the simple behavior described above is modified. The orientation is then set not only by where the electric density is highest, it is also set by where the flux escapes. As a consequence it is possible to have the polarization switch sign, and, when the continuous absorption and emissivity is important, the sign

can also be wavelength dependent. For an axisymmetric system, the polarization is always perpendicular or parallel to the symmetry axis (since these are the only unique directions). Thus, when there is wavelength dependence in the polarization, a signature of switching from pole-dominated to equator-dominated polarization is a 90 degree rotation in the polarization position angle. By contrast, a switch from intrinsic-dominated to ISM-dominated polarization can be a rotation of the polarization through any position angle.

Line emission offers another probe. For recombination lines it is typically assumed that the emission is unpolarized. Also, some resonance lines are at least partially depolarizing. Consequently line photons, which originate at larger distances in the envelope, will (at least for the optically thin case) show less polarization than the adjacent continuum.

Our view of the mass transfer process in OB interacting binaries was substantially refined by the pioneering high-resolution FUV spectroscopic observations from the *IUE* and *FUSE* spacecraft (https://archive.stsci.edu/iue/; https://archive.stsci.edu/fuse/). Circumstellar (CS) material was not only in accretion disks, but also in *splash* and other localized outflow regions in the orbital plane, jets that produced mass loss above/below the orbital plane, and high-temperature (10^5 K) plasmas. But limited phase coverage within an orbital cycle compromised our ability to map these structures and it was difficult to detect outflows above/below the orbital plane (jets) unless the system displayed a total eclipse. Mass loss from the system during the mass transfer phase was difficult to quantify.

In this paper, we consider how the spectroscopic and polarimetric diagnostics of mass streams and circumstellar disks can reveal the fraction of material that escapes from the system. We begin in Section 2 with a discussion of well-known systems, viewed through their location in the r-q diagram. The latter is of great importance to our objective of understanding the evolution of mass transfer binaries that are predominantly B-type systems as they provide a statistically significant sample. Then in Section 3 we lay out the details of the *Polstar* observational scheme, establishing the required observational requirements and connecting them to *Polstar's* projected capabilities, to build confidence in the success of an experiment that combines polarimetry, spectroscopy, and light curve information as a function of orbital phase. Section 4 continues with a discussion of how polarimetry can be used to infer the mass flow structures in interacting binaries, potentially containing disks and jets, given their importance for understanding the conservative and nonconservative elements of the mass transfer budget. This section concludes with an application to the well-known B-type binary β Lyrae from polarimetric data secured from ground-based instrumentation and FUV spectrophotometry from the spacecraft *WUPPE*. Section 5 describes the spectroscopic signatures of mass flow, which crucially complements the polarimetric information because of its quantitative velocity and geometrical constraints on mass streams, splash zones, high-temperature accretion regions, and plasma jets. Concluding remarks are given in Section 6.

2 The Interacting Binary Landscape

The importance of binarity on the evolution of OB stars and where the Be stars fit into the picture has been discussed since the mid-1970s (Kriz and Harmanec, 1975; Plavec and Polidan, 1976; Plavec, 1976). The fate of a B star depends on how close it is to its nearest neighbor when it reaches the main sequence. If the separation of the binary components is small enough, at some point during its post main sequence ($PoMS$) evolution the more massive component will have a radius that is equal to the mean radius of its Roche surface[1]. Transfer of material from the latter star to its companion will commence during one of the major $PoMS$ expansion phases (Plavec, 1970) depending on the initial binary separation: 1) during main sequence expansion (Case A), 2) on the subgiant branch (Case B), or 3) on the asymptotic giant branch (Case C). Although several subgroups of early-type interacting binaries can be associated with the evolutionary groups mentioned above, here we focus on the B-type near contact systems (initial periods up to $\lesssim 1.5^{\rm d}$) and the Algol-type binaries (initial periods from $1.5^{\rm d} \lesssim {\rm P} \lesssim 60^{\rm d}$, if the mass loser was originally about $5{\rm M}_\odot$ and the mass ratio

[1]These systems are often called *close binaries*.

0.3). Typically the contact systems are associated with Case A or slightly beyond and the Algols are usually Case B mass transfer.

The early calculations on the evolution of close binaries were invariably based upon conservative mass transfer in which all the mass that was lost from the donor star ended up being accreted by the mass-gaining star. The consensus now is that significant mass and angular momentum is indeed lost from the system. The primary objective of this investigation is to identify the stages of mass transfer during which most mass is lost and measure it from phase-dependent FUV spectroscopy and spectropolarimetry.

Lubow and Shu (1975, 1976) provided us with our first basic understanding on how a localized stellar wind at a binary's inner Lagrangian point, L1, becomes a defined gas stream that either impacts the mass-gaining star[2] or feeds an accretion disk around it. The nature of the CS structures in interacting binaries can be understood with the aid of the *r-q* diagram in which the fractional radius of the mass gainer (R_p/a) is plotted versus the mass ratio, $q = M_{loser}/M_{gainer}$, and compared with the theoretical computations of gas stream hydrodynamics of Lubow and Shu (1975). Such a display is presented in Figure 1. The upper *dashed* curve, ϖ_d, delineates the fractional radius of the dense accretion disk for systems of different mass ratios. The lower *dashed* curve, ϖ_{min}, shows the minimum distance that a stream particle will achieve relative to the center of the gainer. If the system falls above the upper curve (henceforth called *Region 1*), the gas stream will strike the photosphere of the gainer and any Hα emission seen from the CS material will be transient. These binaries are often called *direct-impact* systems. If the system falls below the lower curve (*Region 3*), then one will see a prominent accretion disk that emits strongly in Hα. The amount of material in the accretion disk can vary, especially for systems near the lower curve. The most variable accretion disks are found in systems that fall between the two curves (*Region 2*) where the gas stream impact is nearly tangential. The inner part of a wide gas stream will strike or graze the photosphere of the primary while the outer edge will feed an accretion disk. For the systems plotted in Figure 1 above the ϖ_{min} line, the angle between the impacting gas stream and the photosphere of the B star varies from $\sim 50^o$ (e.g. Z Vul) to tangential (e.g. V393 Sco, V356 Sgr).

After its onset, mass transfer proceeds on a fast timescale until the masses of both stars are the same (Plavec, 1970). If mass and angular momentum were to be conserved, the orbital period and binary separation would steadily decrease, which would cause a runaway that would likely violate the conservative assumptions. Hence we expect substantial mass to be lost from the system at this stage. All or some of the systems may experience Common Envelope Evolution (Ivanova et al, 2013) during their pre-mass reversal stage, but more studies are needed to understand this phase.

There are very few recognized examples of pre-mass reversal objects. We consider three such systems here: SX Aur (Linnell et al, 1988), SV Cen (Drechsel et al, 1982; Linnell and Scheick, 1991), and UX Mon (Sudar et al, 2011). The radius of the primary component in the SX Aur system is quite close to being in contact with its Roche surface, while its companion is unevolved. This system appears to be on the verge of beginning the mass transfer process. Although the more massive star did not show any obvious evidence of CS material in the *IUE* spectra, an image from the WISE spacecraft (Deschamps et al, 2015) clearly reveals evidence of earlier mass loss.

SV Cen and UX Mon are definitely in the pre-mass reversal phase. SV Cen is distinguished by displaying the fastest known rate of period decrease, ($\dot{P}/P \approx -1.5 \cdot 10^{-5}$ yr^{-1}, Drechsel and Lorenz, 1993). From 1894 to 1993 the period shortened on the average by 2.2 s yr^{-1}, indicating a mass transfer rate of 4×10^{-4} $M_\odot$ yr^{-1}. Drechsel et al (1982) report systemic mass loss in SV Cen from the analysis of *IUE* spectra. UX Mon currently shows a decreasing orbital period of $\dot{P} = -0.260$ s yr^{-1} (Sudar et al, 2011). The primary may be embedded in an optically-thick accretion disk and the system seems to be related to the W Serpentis binaries.

All of the Algol binaries shown in Figure 1 were observed with *IUE*, except the O-type system XZ Cep. Some observational details are highlighted in Section 5. The mass gainers for all of the Algol binaries plotted in Regions 2 and 3 are rotating supersynchronously, as are about half of

[2]In contemporary terminology the star that is losing mass is often called simply the *loser* and the mass-gaining star the *gainer*.

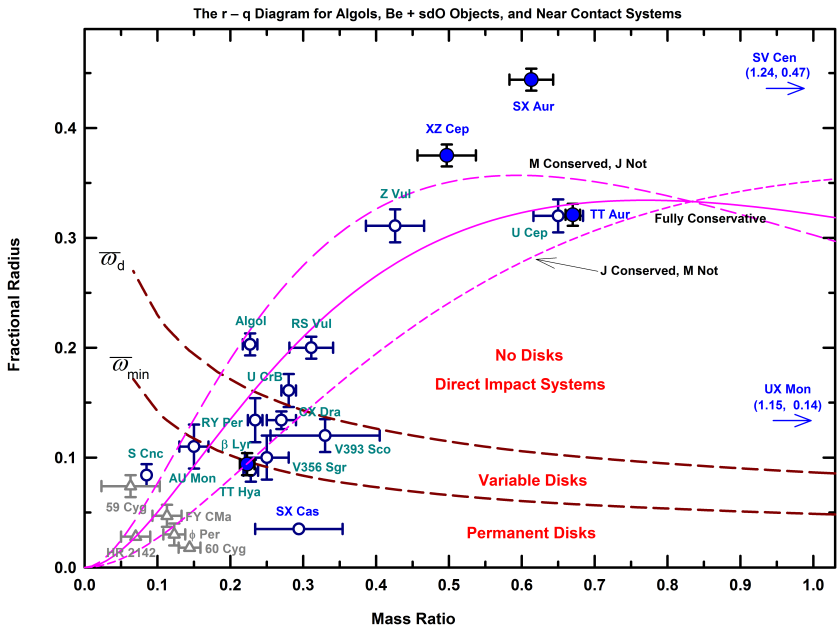

Fig. 1 The locations of targets selected for this study (cf. Section 3) in the *r*-*q* diagram. The near contact systems are plotted with *solid blue* circles, while the Algol binaries are indicated by *open* circles and *cyan* labels. The objects plotted with *open gray triangles* are Be +sdO systems. The error bars are from individual papers on each star. The *magenta* long-dashed and short-dashed curves indicate, respectively, trajectories of predominantly nonconserved angular momentum and nonconserved mass transfer, as discussed in the text. The evolutionary track for fully conservative mass transfer is shown by the solid *magenta* curve.

the systems in Region 1. This is not a surprise because the gas stream is impacting the gainer's photosphere or inner disk with a velocity of about 400 km s^{-1}. It is thought that the systems that are tidally-locked are experiencing a hiatus in the flow of the gas stream. Considering the high velocity of the gas stream, if the impact is tangential one might expect that the material in the flow will head out of the system near phase 0.5 and be lost to the ISM. In fact this is observed: see the discussion of the UV spectropolarimetry of β Lyr from *WUPPE* (Hoffman et al, 1998; Harmanec et al, 1996) discussed in Section 4.

The five longest known Be + sdO (BeS) systems, which are in a post-interaction stage, are seen in the lower left-hand corner of the *r*-*q* diagram in Figure 1. These systems are relevant to the *Polstar* objective *S4* as providing context for the final stages of a nonconservative transfer process happening earlier, but they are also relevant to another objective, *S3*, which tests the hypothesis that classical Be stars are a post mass transfer stage that eventually produces a BeS object (Jones et al, 2022). The sdO objects (cf., Wang et al, 2021, and references therein) are thought to be the stripped down, CNO processed core of a mass loser that transferred significant mass and angular momentum to the Be star. Consider the following scenario. If the mass from the loser arrives with too much angular momentum, it must shed some of its extra angular momentum to allow for more accretion without overloading the gainer. Recall from discussion above that the component separation and orbital period of mass-transferring binary steadily decreases until the mass ratio is 1.0. After the mass reversal, the opposite happens.

There is an initial rapid and unstable mass transfer that could have significant mass loss, and then later once stability sets in and both stars thermally equilibrate, we have transverse mass streams and a second phase of mass loss during region 2. As the system enters Region 3 the excess

angular momentum spins up the gainer (at least its upper envelope and photosphere) and transfers it to a disk structure. The accretion disk material loses energy due to viscosity, so it falls to the photosphere, while the angular momentum is transported outward by viscosity and may contribute to an unstable decretion (mass loss) disk.

This continues as the mass loser shrinks below its Roche surface and exposes its core. Since the Be star in the known bright BeS systems typically has a mass $> 8{-}9 M_\odot$, and the sdO object is $\approx 1.5\ M_\odot$, if there is substantial systemic mass loss, the original mass loser and current sdO was probably a late O-star. More information on the sdO objects and their associated Be stars can be found in Jones et al. 2022 (this Topical Collection).

The spinup of the gainer requires only a small amount of angular momentum. The lions share is locked in the binary orbit, and our current purpose is to understand how much of that angular momentum and total mass is lost from the system during interaction. For this, we focus on the nonconservative interaction phases alluded to above, and their immediate aftermath. To focus our attention on the possibilities, there are three theoretical trajectories that curve from the upper right to the lower left in Figure 1. The central trajectory is for conservation of both mass and angular momentum, taking as an example a ratio of gainer radius to orbital separation at mass reversal ($q = 1$) of 1/3. Note that the largest possible value of this ratio at $q = 1$ is 1/2, because otherwise both stars would need to fill their Roche lobes at mass reversal, and the assumption is that only the mass loser is undergoing Roche lobe overflow. Hence the central trajectory is already a fairly aggressive assumption about how large R/a can be without angular momentum loss from the system. The *long-dashed* trajectory assumes that no significant mass is lost from the system, but no angular momentum transfer occurs (simulating a limit where the minority of the mass carries off the majority of the angular momentum, such as for a decretion disk). Loss of orbital angular momentum causes the system to spiral inward toward lower separation a, raising r/a as shown in Figure 1. Hence the systems found at high levels of r/a are likely to require angular momentum loss.

Conversely, the *short-dashed* trajectory below the conservative one assumes the mass is completely lost from the system, but completely conservative angular momentum transfer is occurring (simulating a limit of mass jets being lost that carry little angular momentum). Loss of mass causes the system to spiral outward toward higher separation a, lowering r/a. Hence the systems found at low levels of r/a are likely to have experienced significant mass loss without significant angular momentum loss.

The figure suggests that both types of nonconservative evolution might be occurring in different systems, but this is somewhat ambiguous because we do not know the history of the systems. We do not know the values of their r/a when q equaled 1.0. However, what is clear is that the systems with the highest r/a must have required angular momentum loss, because their conservative trajectory would track back to $r/a > 1/2$ at $q = 1$, which is not possible given the assumptions about the mass transfer process as mentioned above. Given that mass loss that carries a large amount of angular momentum, as well as mass loss that carries only a small amount, are both potentially playing out in these systems, we wish to watch all these systems carefully, both spectrally and polarimetrically, at multiple orbital phases, to look for signatures of either geometry of nonconservative mass transfer in the experiment described next.

3 Proposed Observing Program and Target List

The *Polstar* observing strategy, instrument requirements, and projected performance is described in this section, as well as the target list (cf. Table 1) that gives sufficient coverage of key systems to achieve the objective denoted *S4*. This objective is to look for spectropolarimetric evidence in currently interacting binaries that can test the hypothesis that mass transfer is significantly nonconservative in its early and rapid phases prior to and shortly following mass reversal. The strategy involves 20 visits (10 for the dimmest targets), mostly spread evenly over the phase of the binary orbit but with a few extra visits over the eclipse phase for those systems that do eclipse. The plan is to combine spectroscopic searches to resolve absorption lines from mass

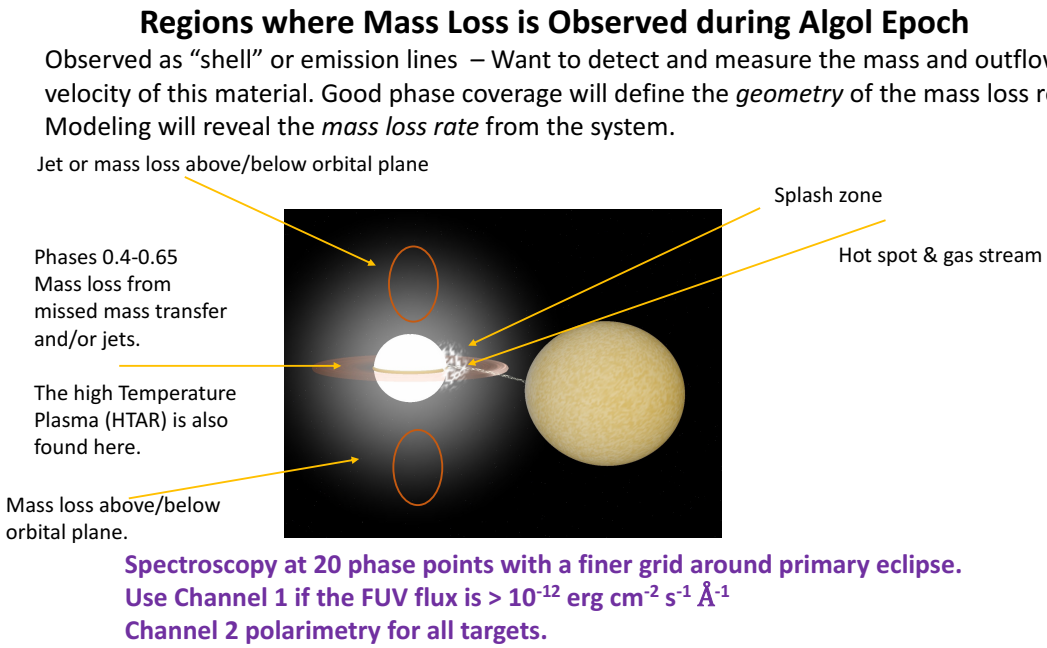

Fig. 2 Circumstellar gas/plasma structures observed in Algol-type binaries. All have been inferred from phase-dependent FUV spectral lines and polarimetric signatures.

streams seen in projection against the face of the primary gainer, with polarimetric data capable of exposing the presence of free-electron scattering well away from the face of the star. In this way, both the mass transfer rate can be characterized (spectroscopically), as well as the rate of escaping mass (polarimetrically).

Figure 2 shows the locations of the most commonly observed CS structures in mass transfer binaries of the Algol type. The disk parameters are usually determined from modeling hydrogen emission lines (mostly Hα). But all of the other structures have been identified from modeling FUV absorption spectra from *IUE*, *FUSE*, or *HST*. These structures include the gas stream, a hot spot at the impact site, a *splash* plasma, mass outflow near phase 0.5 (superior conjunction of the mass-losing star), jets, and a high-temperature plasma in the equatorial region downstream from the impact location.

To carry out the S4 objective, the spectroscopy must be of high enough resolution to pick out mass streams at speeds of a few hundred km s^{-1}, given that the projection toward our line of sight might be smaller. Many data points are needed across the profiles to study their shape. Opacity in key resonance lines such as C IV at 155 nm and N V at 124 nm is high, as the strength of the resonance compensates for low abundance. Hence if about 10 data points can be placed across a transient absorption profile that appears cyclically with orbital phase, with a resolution of about $R \cong 30,000$ one can find the nature of a mass transfer flow from spectroscopy. Since the mass transfer rate is high and the infalling velocity gradient weak, strong UV resonance lines in the stream will be optically thick. But since the Roche lobe overflow region is expected to be rather compact, the stream may not cover a large fraction of the face of the mass gainer, as Figure 1 shows, so that the gainer may fill a significant fraction of the interbinary separation. Relatively high SNR ($> 50 - 100$) is therefore expected to be required to quantify the highly unsaturated depth of the absorption by the mass stream in each $\cong$ 10 km s^{-1} resolution element, when it is caught in projection against the stellar disk. To assist with this desired geometry, high inclination (often eclipsing) systems are chosen in the target list. In all, the instrument requirements to carry out the spectroscopy of objective *S4* are set at $R = 30{,}000$ and $S/N = 50$-100.

The required polarization precision is set at 1×10^{-3}, with the expectation that nonconservative mass transfer will be indicated by a highly asymmetric geometry of escaping mass. Systems shown in Figure 1 that exhibit surprisingly wide separations may require an excess of mass loss over angular momentum loss to achieve such wide separations (as suggested by the short-dashed curve). These systems could be expected to exhibit mass loss from the system in polar directions, as shown in Figure 2. Polarization with a position angle aligned with the orbital plane can be anticipated from these systems if the *S4* hypothesis is correct.

Conversely, systems from Figure 1 that exhibit surprisingly small separations may require high angular momentum loss relative to mass loss, to cause the orbit to spiral inward suitably to explain their position in the r-q diagram. These latter systems could be expected to exhibit mass loss from the system in the equatorial plane, seen spectroscopically as blueshifted "shell" lines at orbital phases where they cross the stellar disk, and associated with a polarization position angle that is perpendicular to the plane of the orbit.

Since the optical depth of the free-electron scattering responsible for this continuum polarization is significantly less than the optical depth in strong UV resonance lines, yet the mass flux of significantly nonconservative transfer would rival that of the mass transfer rate, the free-electron optical depth is expected to be substantial, perhaps comparable to free-electron optical depths (~ 0.1) in the strongest O-star winds. Such highly aspherical free electron structures would induce polarized scattering, but at a significantly reduced level from their optical depths, so we set the required polarization precision necessary to detect these escaping mass streams at 1×10^{-3}. This strategy takes advantage of the fact that Ch2 has a roughly factor 3 advantage in effective area over Ch1, such that a factor 2.5 increase in photon count is achieved by only a factor 1.5 increase in total exposure time per visit. It also allows us to monitor in real time the consistency between the channels.

To establish that the projected performance of the *Polstar* experiment can meet these requirements, the target list in Table 1 shows the required exposure times in Ch1 needed to achieve the listed S/N and the precision in Ch2 for each visit and the number of phase points to be covered. The strategy for determining the indicated polarization precision involves combining each Ch1 exposure with a Ch2 exposure of half the Ch1 exposure time. This takes advantage of the fact that Ch2 has an effective area that is about a factor of three over Ch1, such that a factor 2.5 increase in photon count is achieved by only a factor 1.5 increase in total exposure time per visit. This is deemed a useful strategy for helping to build the stringent polarization precision desired, and is included in the calculation of the indicated polarization precision in the final column. We see from Table 1 that the instrument requirements are met with margin by these projected performance benchmarks. The total observing time implicit in the observing strategy is 27 days, an acceptable resource allocation for one of twelve objectives of *Polstar* in a 3-year mission timeline, while still accounting for a 50% duty cycle, as well as potential time set aside for a guest observing program.

4 Polarimetry of Interacting Binaries with Disks

4.1 Basics of polarimetric behavior

There is a suite of modeling tools, such as Monte Carlo radiative transfer (Whitney et al, 2017; Carciofi et al, 2017; Shrestha et al, 2018), for evaluating polarization from binaries in optically thin or thick regimes. It is however useful to explore the thin scattering regime, particularly the theory advanced by Brown et al (1978). While thin scattering can be limited in providing quantitatively accurate results Wood et al (e.g., 1996), it can often provide appropriate order of magnitude results and especially insights into qualitative behavior. Moreover, owing to the low value of the Thomson scattering cross-section, there are many applications in which thin scattering applies at the densities representative of some circumstellar media.

Here we review the Brown et al (1978) approach for a binary system using somewhat modified notation and presentation that draws partly on Brown et al (1978) and partly on Brown et al (1982). The Brown et al (1978) approaches makes several simplifying assumptions such as point source illumination, neglect of occultation

Table 1 Target List

HD Number	Star Name	Spectral Types	System Type*	Period in days	UV Flux in erg cm^{-2} s^{-1} Å^{-1} (channel)	Exposure Time in Ch1 (s)	Number of phases	SNR in Ch1	Precision in Ch2 (10^{-3})
5679	U Cep	B8Ve + G8IV	A	2.493	1.00x10^{-11} (1) 1.20x10^{-11} (2)	5000	20	100	0.5
10516	ϕ Per	B1.5e + sdO	BeS	126.673	1.50x10^{-09} (1) 1.50x10^{-09} (2)	600	20	400	0.3
17034	RY Per	B3Ve + F7II-III	A	6.864	4.00x10^{-12} (1) 3.00x10^{-12} (2)	6000	10	70	0.7
19356	Algol	B8V + K2IV	A	2.867	3.00x10^{-09} (1) 3.00x10^{-09} (2)	600	20	600	0.2
33088	TT Aur	B2V + B4IV	EC	1.333	1.00x10^{-11} (1) 5.00x10^{-12} (2)	3000	20	80	0.9
33357	SX Aur	B1.5V + B3V	EC	1.210	2.00x10^{-11} (1) 6.00x10^{-12} (2)	2500	20	100	0.9
41335	HR 2142	B1.5Ve + sdO	BeS	80.913	4.00x10^{-10} (1) 2.00x10^{-10} (2)	200	20	120	0.6
50846	AU Mon	B3Ve + F8III	A	11.113	1.50x10^{-11} (1) 4.00x10^{-12} (2)	3600	20	100	0.8
58978	FY CMa	B0.5Ve + sdO	BeS	37.257	6.00x10^{-10} (1) 6.00x10^{-10} (2)	600	20	250	0.3
65607	UX Mon	A5Ve + G2III	A	5.904	1.00x10^{-12} (1) 1.00x10^{-12} (2)	30000	10	80	0.6
74307	S Cnc	B9.5V + G8IV	A	9.485	4.00x10^{-12} (1) 4.00x10^{-12} (2)	6000	10	70	0.6
97528	TT Hya	B9.5Ve + K3IV	A	6.953	9.00x10^{-12} (1) 4.00x10^{-12} (2)	4000	10	80	0.7
102552	SV Cen	B1V + B6.5III	EC	1.658	6.00x10^{-12} (1) 4.00x10^{-12} (2)	6000	10	80	0.7
136175	U CrB	B6V + F8III-IV	A	3.452	2.00x10^{-11} (1) 4.00x10^{-12} (2)	2500	20	100	0.7
155550	FV Sco	B4IV + F-G:	A	5.727	1.50x10^{-11} (1) 5.00x10^{-12} (2)	4000	10	100	0.6
161741	V393 Sco	B3V + A:	A	7.713	1.50x10^{-11} (1) 8.00x10^{-12} (2)	4000	10	100	0.7
173787	V356 Sgr	B3V + A2II	A	8.896	4.00x10^{-12} (1) 7.00x10^{-12} (2)	6000	10	70	0.5
174237	CX Dra	B2.5Ve + F5III	A	6.696	2.00x10^{-10} (1) 8.00x10^{-11} (2)	900	20	200	0.5
180939	RS Vul	B5V + G1III	A	4.478	3.00x10^{-11} (1) 1.30x10^{-11} (2)	2000	20	100	0.6
181987	Z Vul	B3V + AIII	A	2.455	2.00x10^{-11} (1) 3.10x10^{-11} (2)	2500	20	100	0.4
200120	59 Cyg	B1Ve + sdO	BeS	28.187	1.10x10^{-09} (1) 1.10x10^{-09} (1)	600	20	350	0.3
200310	60 Cyg	B1Ve + sdO	BeS	146.6	5.00x10^{-10} (1) 1.70x10^{-10} (2)	600	20	200	0.5
	XZ Cep	O9.5V + B1III	O	5.1		3600	20	100	1
232121	SX Cas	B5Ve + K3III	W	36.561	4.00x10^{-13} (1) 1.00x10^{-13} (2)	30000	10	50	1

*A=Algol, BeS=Be+sdO, EC = Early-Type Contact,O=O-type system, W=W Ser.

effects, no reflections off either star, and thin scattering as already noted. The authors then proceed to define distributions of the scattering envelope as weighted essentially by lower-term spherical harmonics (e.g., Simmons, 1982, 1983). There are three broad classifications of these moments: overall asphericity, left-right asymmetry, and front-back asymmetry. Overall asphericity is in relation to the orbital plane of the binary; left-right is respect to the line-of-centers (LOC) joining the two stellar components; and back-front is with respect to each star.

As an example, consider the representative schematics of Figure 3. Top shows a single isotropic point source with a circumstellar disk. This is aspherical and yields a net polarization when the disk is spatially unresolved. As long as the disk is steady-state (i.e., no change of the axisymmetric structure or optical depth), the polarization is constant. The disk is viewed at

some inclination, certainly not pole-on but neither edge-on, and the net polarization would be negative by convention: the net polarization would be oriented with the symmetry axis of the disk.

Allowing for finite stellar size of the star (2nd schematic from top) leads to occultation, which can alter the level of net polarization. Although occultation is not treated by Brown et al (1978), the topic has been considered by several authors (e.g., Fox, 1991). The effect of a finite sized star induces no time variable polarization as long as the disk is steady. Indeed, even if the star itself is variable, the polarization will remain constant being a ratio of polarized flux to total flux.

In the next schematic (3rd from top), a binary companion is added (referring to it as the secondary, whereas the star with disk is the primary), and the polarization becomes time-dependent and cyclical with orbital phase. Even if the disk is steady-state, both the polarization and position angle (PA) can change as the secondary orbits the primary, owing to the changing orientation of how starlight is scattered into the observer sightline. Relative to the secondary, the disk represents a front-back asymmetry for the scattering distribution, but not left-right asymmetry.

The bottom schematic in Figure 3 is another scenario not treated by Brown et al (1978). In this case the system's inclination is large enough for secondary star to eclipse both the primary and the disk. This is shown for two reasons. First, several targets for *Polstar* are close eclipsing binaries and eclipses contain a wealth of diagnostic material involving both spectral line and continuum polarization for extracting the geometry of the binary system. Although Brown et al (1978) only deals with point sources, this last schematic also highlight how in a close binary, one expects accretion and thus an accretion stream. Indeed one may even expect a hot spot on the disk where mass from the stream enters the disk (e.g., Lomax et al, 2012b). Although the schematic does not include a stream or hot spot, these have two main effects.

First, one can easily imagine that the stream creates a break in left-right symmetry about the LOC between the stars. This introduces a lead-lag effect in the polarized light curve relative to eclipsing light curve. Second, a hot spot will have a spectrum, representing a third source of illumination for scattering by electrons in the ionized envelope. The approach of Brown et al (1978) allows for any number of illuminating sources to explore such effects, especially wavelength-dependence.

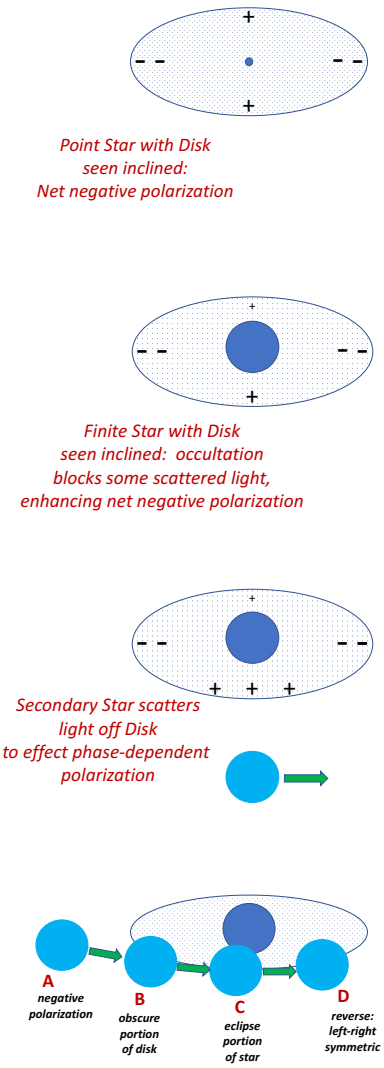

Fig. 3 Schematic representation for four scenarios producing constant or time variable linear polarization, as discussed in text. Top is an axisymmetric disk around a point star. Next down is the same disk with a finite sized star. Third is the addition of an orbiting companion star. Bottom is a higher inclination scenario of relevance for many close binary targets of *Polstar* involving eclipse effects.

Note that orbital eccentricity can also introduce new effects (e.g., Brown et al, 1982; Manset and Bastien, 2000), but for relatively close and typically interacting binaries, we shall assume circular orbits in presenting heuristic models to illustrate (a) how geometry is extracted from variable continuum polarimetry and (b) chromatic effects in the UV that may improve defining the geometry based on the data.

Monte Carlo radiative transfer approaches are capable of taking into account the many realistic factors that influence variable polarization from interacting binaries: the effects of finite stellar size for eclipses and occultation, the effects of multiple scattering, the effects multiple components such as a hot spot or accretion stream. However, for purposes of illustrating the essentials of modeling polarimetric variability from hot star binaries, and in particular the expectation of chromatic effects in the UV band observable with *Polstar*, an example is developed using the approach of Brown et al (1978). Following that paper, adopting some notation from Brown et al (1982), and modifying it slightly, the linear polarization in Stokes-Q and Stokes-U for a binary with a circular orbit is given by

$$\begin{aligned} q &= \bar{\tau} - 3\tau_0 \sin^2 i + G \sin 2i \, \cos(\phi + \phi_G) \\ &\quad -H(1 + \cos^2 i) \, \cos[2(\phi + \phi_H)] \qquad (1) \\ u &= 2G \sin i \, \sin(\phi + \phi_G) \\ &\quad -2H \cos i \, \sin[2(\phi + \phi_H)], \qquad (2) \end{aligned}$$

where i is the viewing inclination (such that $i = 0°$ is a top-down view of the orbit) and ϕ is the azimuth of the LOC in the orbit plane, relative to the viewer sightline. The coefficients G and H are given in Brown et al (1982), where G contains terms that are left-right asymmetric, but also top-down asymmetric, while H contains terms that are left-right asymmetric and back-front asymmetric. We will assume that the scattering distribution is top-down symmetric, so $G = 0$. As a result q has a constant term and time or phase dependent term with pattern variation of twice per orbit and potential phase lag signified by ϕ_H. Then u is similar but with no constant term. The polarimetric variation in a $q - u$ diagram is an elliptical figure based on the variable terms, with two circuits about the ellipse in one orbit, and a constant offset in the direction of q. The eccentricity of the ellipse relates to the viewing inclination, with circular for $i = 0°$ and degenerating to a line for $i = 90°$ (since u would be zero).

Definitions for the remaining parameters are:

$$\begin{aligned} H^2 &= \tau_3^2 + \tau_4^2 \qquad (3) \\ \tan 2\phi_H &= \tau_4/\tau_3 \qquad (4) \\ \bar{\tau} &= f_1(\lambda)\bar{\tau}_1 + f_2(\lambda)\bar{\tau}_2 \qquad (5) \\ \tau_0 &= f_1(\lambda)\tau_{01} + f_2(\lambda)\tau_{02} \qquad (6) \\ \tau_3 &= f_1(\lambda)\tau_{31} + f_2(\lambda)\tau_{32} \qquad (7) \\ \tau_4 &= f_1(\lambda)\tau_{41} + f_2(\lambda)\tau_{42}. \qquad (8) \end{aligned}$$

where f_1 and f_2 are the relative monochromatic luminosities of the respective stars (1 for primary and 2 for secondary) as fractions of the total: $f_1 = L_1/(L_1 + L_2)$ and $f_2 = L_2/(L_1 + L_2)$. As will be addressed shortly, it is these terms that can allow for chromatic effects despite electron scattering being a gray opacity. For the various τ parameters at left, the additional subscript of 1 or 2 for terms on the right signify moment calculations of the scattering distribution relative to the respective stars. Note that symbol "τ" is chosen because those factors scale as optical depths. Each one scales as the product $n_0\sigma_T L$, for n_0 a characteristic number density of electrons, σ_T the Thomson cross-section, and L a characteristic length. And this holds for the various defined components in the system, such as a disk, an accretion stream, a jet, or a wind. The definitions of the τ terms can be found in BME in terms of the integral relations (although those authors refer to shape factors γ, but the integrals are the same).

The offset term involving $\bar{\tau}$ and τ_0 does not contribute to variable polarization. It is an offset, and without additional information, might not be easily disentangled from the ISP, unless the Serkowski fit (e.g., Taylor et al, 1991; Clayton et al, 1992) is quite well determined. Note that the offset can show chromatic effects in the UV, to be addressed later. It is however the variable polarization that can be straightforwardly attributed to the binary as distinct from the interstellar contribution. Consequently, we ignore the offset in the discussion that follows, although the offset contains additional useful information about the

geometry of the stellar system if it can be disentangled from the ISM polarization (e.g., Nordsieck et al, 2001).

Now to address chromatic effects that have been mentioned several times. The two fractions f_1 and f_2 are wavelength dependent. Since the focus is on hot massive stars, in the optical and IR band, the continua spectra of both stars will be approximately Rayleigh-Jeans. As a result, both f_1 and f_2 become constant, as the λ^{-4} factor cancels. Consequently, the polarization is flat across those spectral bands. (The polarization is also flat if one star dominates the luminosity at every wavelength of observation.)

However, in the UV, the two stars will generally have different temperatures and therefore different Wien peaks. The different temperatures and different radii of the stars mean that f_1 and f_2 also become wavelength-dependent, such that the luminosity weighted terms contribute to q and u to produce polarization with chromatic effects (i.e., not flat polarized spectra). The chromatic effects emphasize certain moment terms that better define the geometry of the system in relation to model fitting. In particular, the phase lead-lag (ϕ_H) is itself chromatic, a strong constraint on geometrical components in the spatially unresolved system. Note that the moment terms expressed as the τ parameters are not chromatic but are fixed by the geometry of the system; it is only the weighted sums that are chromatic by virtue of the two different stellar spectral distributions.

For a simple illustration, Figure 4 shows results using the preceding expressions for a binary involving a primary star surrounded by an axisymmetric disk; see schematic to scale at top. The primary is hotter and smaller; the secondary is cooler and larger, with parameter values specified in the schematic. The inclination is about 72° ($\cos i = 0.3$). Polarimetric variability is displayed in the middle panel with colors as specified in the label for q, u, and $p = \sqrt{q^2 + u^2}$. Finally at bottom is shown the position angle (PA) variation. Both middle and bottom are plotted with orbital phase, ranging from 0 to 1. At phase zero, the secondary would be forefront if seen edge-on.

Several key points are noted. First the various curves in the middle panel are for different wavelengths of 100 nm to 400 nm in equal steps. For sake of illustration, the stellar spectra of the

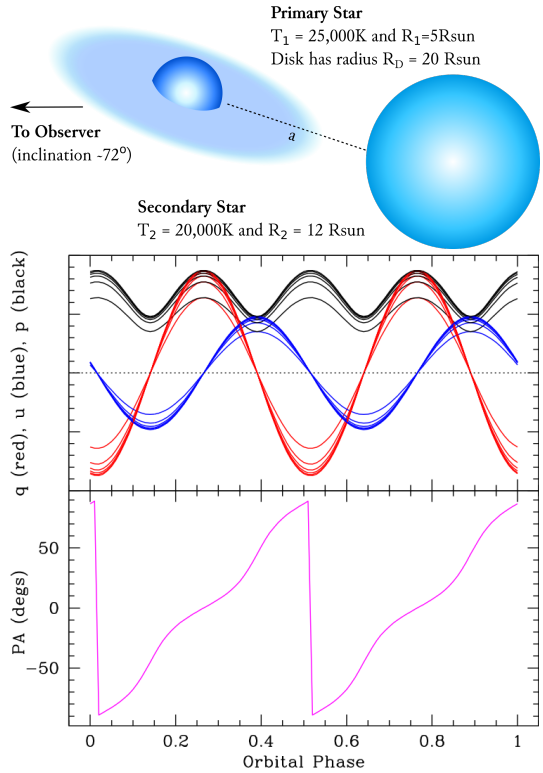

Fig. 4 Three panels as illustration of polarimetric variability for a binary system. Top: A cartoon to depict a primary surrounded by an axisymmetric disk orbited by a secondary star with temperatures and sizes indicated. Middle: Variation of q, u, and $p = \sqrt{q^2 + u^2}$ with colors indicated in the label. Note that the different curves are for different wavelength, from 100nm (smallest p) to 400nm (highest p). The variation arises entirely from scattered light by the secondary star, since the disk is axisymmetric about the primary. Bottom: The position angle (PA) changes with orbital phase. Note that in this model there is no phase lag, for any wavelength, because the system is left-right symmetric; the presence of an accretion stream could change that.

two stars are taken as Planckian at the indicated temperatures. For the selected parameters, the lowest polarization is for 100 nm, and highest for 400 nm. Note how the curves get closer together with increasing wavelength as the individual stars begin to approach their respective Rayleigh-Jeans spectral distributions, just as expected.

Also, the middle panel has no scale provided. The polarization from thin scattering scales with the optical depth of the medium. We can expect amplitude levels for p at 10^{-4} to 10^{-3} fractional polarizations. But p is positive definite, whereas q and u are signed. For edge-on systems we expect $u = 0$, and q varies between $\pm p$, implying a factor

of 2 gain in relative change of polarization, a gain for detection and monitoring purposes.

For the bottom panel, the PA indeed shows cyclic variations at twice the rate of the orbital period. This occurs because the geometry is left-right symmetric. However, whereas the polarization curves in the middle panel show chromatic effects, such effects are absent from the PA variation. This is because there is no left-right asymmetry in the geometry – no accretion stream is included in the model. The accretion stream could introduce a phase lag that is wavelength-dependent. What would that look like? At each wavelength the polarization would trace out an ellipse in the $q-u$ diagram. Each ellipse would be of different sizes for different wavelengths, although the eccentricity would remain constant (since the viewing inclination is constant). The effect of different phase would produce relative rotation shifts between the ellipses.

It is important that the approach of BME can be expanded further to include orbital eccentricity (e.g., colliding wind systems, St-Louis et al, 2022; Ignace et al, 2022) and even a hot spot on the disk. The latter would involve inserting another source of illumination, thus expanding the diversity of chromatic responses. The hot spot will not lie on the LOC of the binary stars, and so would introduce yet an additional phase lag.

The use of BME shows that the UV spectral band is ideal for extracting important information about the geometry of the system, such as symmetry of the disk, or presence of an accretion stream. When used in conjunction with line profile variability, plus the system light curve (most of our targets are eclipsing variables), the scope of the dataset is rich indeed for extracting densities and kinematics of flows, particularly accretion rates, in the system, and additional component representing non-conservative mass-transfer. While BME neglects radiative transfer effects (such as multiple scattering), our team possesses the expertise to model such effects, guided by BME for qualitative behavior and as benchmarks for the detailed codes in the optically thin limit. For example, Hoffman et al (2003) applied MCRT methods to explore the effects of multiple scattering in binary systems that include both interior and exterior disk illumination.

While many of the targets are eclipsing binaries, some are not, and polarimetry can provide a

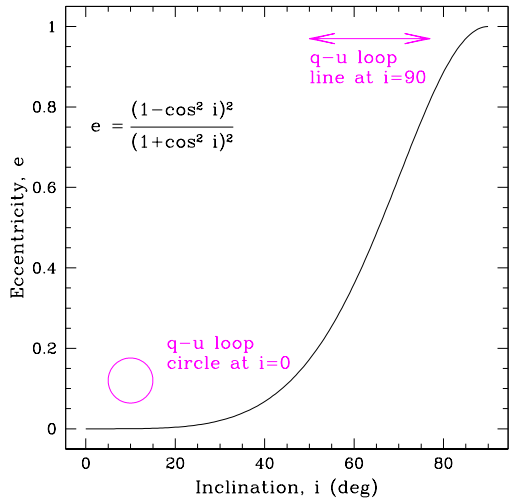

Fig. 5 Eccentricity, e, for the elliptical variations in a $q-u$ diagram for a binary in a circular orbit plotted against viewing inclination, i.

measure (or an additional constraint) to the viewing inclination of the binary orbit. This is important since inclination can often be the greatest ambiguity in the determination of the individual stellar masses. For elliptical variations, the major and minor axes are set by the extrema Δq and Δu, with $e = 1 - (\Delta u^2/\Delta q^2)$. In relation to the viewing inclination:

$$e = \left(\frac{1-\cos^2 i}{1+\cos^2 i}\right)^2 . \tag{9}$$

This relationship is plotted in Figure 5. Note that the error on the measured eccentricity will depend on $\Delta q/\sigma_q$ and $\Delta u/\sigma_u$, for σ_q and σ_u the polarization precision. At high inclination near edge-on, the effort is aided by the fact that the system will be eclipsing. At low inclination, the challenge is the curve is relatively flat below $i \approx 30°$. For fixed measurement uncertainty, the polarimetric variations must be relatively large to distinguish between a $q-u$ loop that is strictly circular (corresponding to pole-on) and one that is only mildly eccentric. Between about 30° to 80°, the relation is more linear.

4.2 Observable signatures of mass loss

UV polarimetry has proven instrumental in detecting the signatures of mass loss from massive interacting binary systems. In the canonical Algol

system β Lyr, Hoffman et al (1998) showed that the near-UV continuum is polarized at 90° to the optical continuum, indicating that two orthogonal scattering regions exist in the system. These authors hypothesized that the PA rotation across the Balmer jump occurs because UV light is preferentially absorbed by the thick disk, so is only seen when it scatters in a perpendicular bipolar flow (Figure 6). This picture was confirmed by interferometric observations (Harmanec et al, 1996; Zhao et al, 2008). By contrast, the similar interacting binary V356 Sgr showed no significant PA difference between the optical and the near-UV (Lomax et al, 2017). This suggests that these Roche-lobe filling binary systems can take on a diversity of geometrical structures, and that using an instrument such as *Polstar* to characterize a broader sample of these objects will allow deeper insights into their physical nature and evolutionary history.

Lomax et al (2012a) used multiwavelength polarimetry to constrain the location and extent of the hot spot on the disk edge in β Lyr; extending this analysis into the UV would provide additional 3-dimensional information about the location of hot gas in this and similar systems. In particular, the light curve of β Lyr is known to be strongly wavelength-dependent, with significant eclipse reversals at shorter wavelengths (Kondo et al, 1994; Ignace et al, 2008), suggesting that time-dependent polarimetric monitoring will open a new, heretofore unexplored window into this and similar systems.

Several of the emission lines in β Lyr show polarization position angles that agree with the UV continuum, suggesting that they scatter primarily from the jet or outflow (Hoffman et al, 1998). In the colliding-wind binary system V444 Cyg, the polarized emission lines probe the stratified layers of the WN star's wind and correlate strongly with the wind geometry as inferred from X-ray emission (Lomax et al, 2015). These findings suggest that the time-dependent line polarization data obtained by *Polstar* will provide detailed information about the structure of the winds in our massive binary targets.

5 Spectroscopic Signatures of Circumstellar Plasma Structures in the FUV

Circumstellar and photospheric structures that have been identified from FUV spectra are shown in Figure 2 and include the gas stream, hot accretion spot, splash plasma, mass loss at phase 0.5 (superior conjunction of the mass loser), jets (mass loss above/below the orbital plane), and a high-temperature plasma (Peters, 2001; Peters and Polidan, 2004).

The gas streams in Algol systems are usually detected from *additional* red-shifted absorption in the moderate-ionization species (e.g. Si II, III, S II, III, Aℓ II, III, Mg II) in the orbital phase interval $0.70 < \phi_o < 0.95$, while enhancements in the mass loss are generally seen from violet-shifted absorption in the Si IV wind lines. An example of gas stream absorption is given in Figure 7. Gas stream signatures can appear either as discrete absorption or an *inverse* wind feature.

Recall that if the system is located in *Region 1* of the *r*-*q* diagram, the mass gainer will present a large enough cross-section that the gas stream will directly impact its photosphere. Since the impact velocity is ~ 400 km s^{-1}, one expects some degree of shock heating at the impact site. Observations of the direct impact system U Cep (P=$2\overset{\mathrm{d}}{.}49$) during the lifetime of the *FUSE* spacecraft present convincing evidence for an accretion hot spot (Peters, 2007). In Figure 8 we show an apparent hot spot rotating into, then out of our line-of-sight. Photometric timing allows one to determine the longitude and size of the hot spot. We estimate that the hot spot is located at the substellar point associated with $0\overset{\mathrm{p}}{.}90$, covers about 2% of the facing photosphere, and has a temperature of $\sim$30000 K which is about three times the $T_{\rm eff}$ of the mass gainer. We plan to look for an elevated FUV flux versus phase in the other *Polstar* targets listed in Table 1 to identify/map hot impact regions in other Algols. The role of hot accretion spots in binary star evolution is discussed by van Rensbergen et al (2008, 2010) who concluded that such spots can help drive mass out of the system and significantly affect the final products of the mass transfer. A likely place to find this type of mass loss would be above/below the orbital plane.

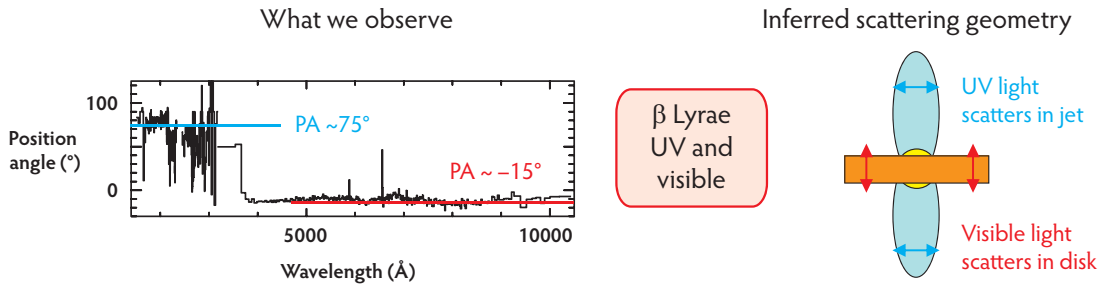

Fig. 6 Polarized spectrum (*left*) of β Lyr and interpretive picture (*right*), based on the study by Hoffman et al (1998). The 90° position angle flip between the near-UV and optical continuum provided key evidence for a jet or outflow in the system oriented orthogonal to the thick accretion disk.

Associated with the accretion spot in U Cep is a localized circumstellar plasma that hovers over the impact region. It is identified from the phase-dependence of the strengths of shell lines of moderate-ionization species. The behavior is shown in Figure 9 in which spectra centered on the Fe III (UV1) resonance multiplet are compared. *Shell-type* absorption features formed in this plasma are observed at phases 0.66, 0.78, and 0.83 but not at phases 0.12, 0.13, and 0.16 even though the hot accretion spot is still visible on the *receding* limb and the FUV flux elevated. Only photospheric lines are observed. When the hot spot is not visible, a pure photospheric spectrum is observed. The localized circumstellar plasma is probably formed as the result of a *splash* associated with the impacting gas stream. The measured velocities of the Fe III shell lines are blue-shifted relative to the photosphere before phase 0.66 but red-shifted in the interval 0.78-0.83. The shell lines from the latter phase interval are apparently formed in the gas stream. Since Fe III and similar

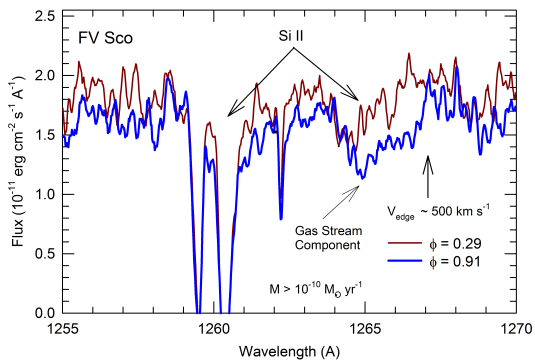

Fig. 7 The Si II resonance lines at 126 nm observed at phases 0.91 & 0.29. Note the red-shifted gas stream component at phase 0.91.

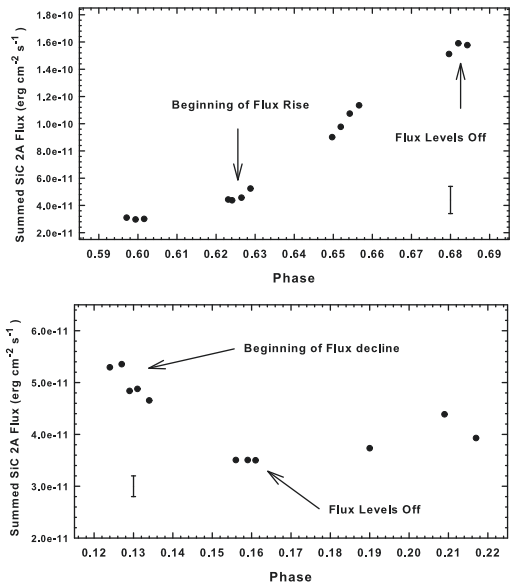

Fig. 8 Evidence for a hot accretion spot in U Cep from *FUSE* data. The summed flux from the SiC 2A detector for each exposure obtained on 2004 February 09 and 2007 March 10 is plotted versus phase. In the *upper* panel note that an apparent hot spot rotates into our line-of-sight at phase 0.625 and is fully visible at phase 0.68. In the *lower* panel we observe this hot spot rotating out of our view a half phase later.

species appear to be dominant, the temperature in the plasma is in the range of 20-40 kK. A splash plasma has also been identified in RY Per (Barai et al, 2004). Hot accretion spots and splash plasmas may be commonplace in Algol binaries. Now that we have observational confirmation of their existence, *Polstar* is poised to yield the data that will allow us to map out the angular extent of such structures and determine how much of the splashed material actually escapes from the system.

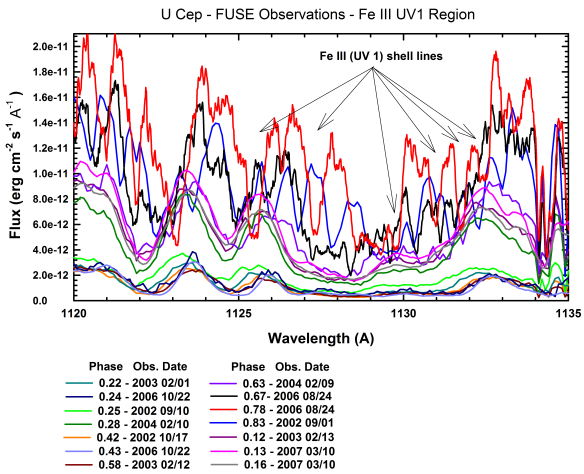

Fig. 9 FUSE spectra of U Cep. Note the elevated flux at phases 0.63, 0.67, 0.78, 0.83, 0.12, 0.13, and 0.16. Obvious "shell" structure is observed at phases 0.66, 0.78, and 0.83, but none at the post-conjunction phases even though the hot spot is still visible. The former suggest outflowing plasma from a splash, region while the latter one reveals infall of material from the gas stream.

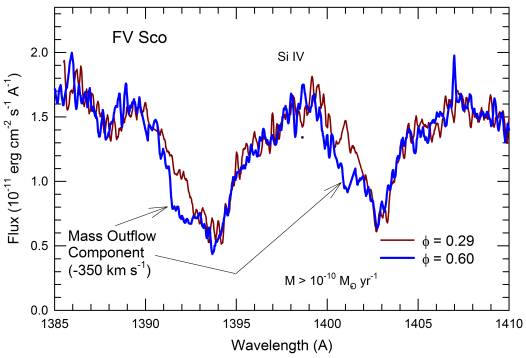

Fig. 10 The Si IV resonance lines at 140 nm observed at phases 0.91 & 0.29. Evidence for extensive mass loss at phase 0.60 is seen from a comparison of the Si IV resonance doublet observed at this phase with a similar observation near quadrature.

Optical and UV studies of Algols have revealed that mass loss near $\phi_o \sim 0.5$ is commonplace Peters (1989, 2001). Often times it is obvious that the flow is a collimated structure caused by the deflection of the gas stream as it impacts the mass gainer's photosphere (cf. Figure 10) at a shallow angle. The mass and angular momentum loss from an Algol system is important for theoretical modeling of its evolution, but this quantity, which remains one of the least known, can be modeled from *Polstar* spectroscopic data through spectrum synthesis techniques. Evolution models with nonconservative mass transfer appear to produce better matches to the observed stellar parameters (e.g., van Rensbergen et al, 2008, 2010; Nelson and Eggleton, 2001). But this is not a new conclusion. About 40 years ago statistical evidence for *extensive* mass loss during the mass transfer was presented by Giuricin and Mardirossian (1981) and Giuricin et al (1983). These authors considered several conservative and nonconservative studies and concluded that mass and angular momentum loss occurred in 20% of their sample.

Jets, or more generally regions of mass loss above/below the orbital plane, may be commonplace in Algol binaries, but they are difficult to detect because most of their material is not along our line-of-sight to the mass gainer. There are both polarimetric (e.g., Hoffman et al, 1998) and FUV spectroscopic (e.g., Peters and Polidan, 2004; Plavec, 1980) signatures. Emission lines are often observed during a total eclipse of the mass gainer. These (usually broad) features are from species of moderate-high ionization. Noteworthy are the O VI and N V resonance doublets that indicate plasma temperatures of 300–100 kK.

The discovery of prominent absorption and emission lines of N V, C IV, and Si IV in the UV spectra of Algol-type binaries in the early 1980s with *IUE* revealed the presence of a high temperature component to the circumstellar material (Peters and Polidan, 1984; Plavec, 1980, 1983). Peters and Polidan called this circumstellar structure the High Temperature Accretion Region (HTAR). They concluded that the HTAR (absorption) lines are formed by resonance scattering in a region of $T_e \sim 10^5$ K, $N_e \sim 10^9$ cm^{-3}, and extreme carbon depletion, C $\sim 10^{-3}$ C$_\odot$. The radial velocity behavior of the UV absorption lines provide compelling evidence that the high temperature plasma is associated with the mass gainer. Since the high temperature plasma appears to be mostly detected on the *trailing* hemisphere of the primary, it was concluded that the plasma producing the HTAR absorption lines is most likely heated by a shock that occurs as the gas stream impacts either the primary's photosphere or inner accretion disk. In some of the systems the material currently being transferred appears to have been processed through the CNO-cycle in the core of the mass loser. Phase-resolved FUV spectroscopy

with *Polstar* will allow us to map the HTAR with more precision and determine if it is an important source of systemic mass loss.

6 Concluding Remarks

In this paper we have discussed how we can quantify the amount of systemic mass loss in OB close binaries from FUV polarimetry and high-resolution spectroscopy with *Polstar*. Since 50-100% of the OB stars are formed with one or more companions, stellar evolution calculations for the upper main sequence must consider mass transfer in close binary systems. We have identified two stages in interacting binary evolution that are important epochs of systemic mass and angular momentum loss: prior to mass reversal and when the system passes through *Region 2* in the *r*-*q* diagram after reversal. We have identified 24 targets that represent all three regions in the *r*-*q* diagram and also have known parameters for their mass gainers and losers as well as the geometry, sizes, and approximate physical conditions in one or more circumstellar structures. With 20 observation pairs (spectroscopy and polarimetry) we will achieve complete phase-coverage with more observations taking place around the eclipse of the mass gainer where mapping of the asymmetrical circumstellar structures will be of high precision. In Section 3 we discussed the observing program in detail and show how we can measure the mass flow and loss in an OB interacting binary with *Polstar* with the necessary signal-to-noise and precision that is needed to quantify the amount of nonconservative mass transfer. Combined with the objectives in *S3* (Jones et al 2022, this Topical Collection) which will address the binary fraction and angular momentum issues, this project will lead to improved evolutionary tracks for OB stars and a more realistic view of their post-main sequence evolution.

References

Astropy Collaboration, Robitaille TP, Tollerud EJ, et al (2013) Astropy: A community Python package for astronomy. A&A558:A33. https://doi.org/10.1051/0004-6361/201322068, https://arxiv.org/abs/arXiv:1307.6212 [astro-ph.IM]

Astropy Collaboration, Price-Whelan AM, Sipőcz BM, et al (2018) The Astropy Project: Building an Open-science Project and Status of the v2.0 Core Package. AJ156(3):123. https://doi.org/10.3847/1538-3881/aabc4f, https://arxiv.org/abs/arXiv:1801.02634 [astro-ph.IM]

Barai P, Gies DR, Choi E, et al (2004) Mass and Angular Momentum Transfer in the Massive Algol Binary RY Persei. ApJ608(2):989–1000. https://doi.org/10.1086/420875, https://arxiv.org/abs/arXiv:astro-ph/0309734 [astro-ph]

Brown JC, McLean IS, Emslie AG (1978) Polarisation by Thomas scattering in optically thin stellar envelopes. II. Binary and multiple star envelopes and the determination of binary inclinations. A&A68:415–427

Brown JC, Aspin C, Simmons JFL, et al (1982) The effect of orbital eccentricity on polarimetric binary diagnostics. MNRAS198:787–794. https://doi.org/10.1093/mnras/198.3.787

Carciofi AC, Bjorkman JE, Zsargó J (2017) HDUST3 - A chemically realistic, 3-D, NLTE radiative transfer code. In: Eldridge JJ, Bray JC, McClelland LAS, et al (eds) The Lives and Death-Throes of Massive Stars, pp 390–390, https://doi.org/10.1017/S1743921317002836

Clayton GC, Anderson CM, Magalhaes AM, et al (1992) The First Spectropolarimetric Study of the Wavelength Dependence of Interstellar Polarization in the Ultraviolet. ApJ385:L53. https://doi.org/10.1086/186276

Deschamps R, Braun K, Jorissen A, et al (2015) Non-conservative evolution in Algols: where is the matter? A&A577:A55. https://doi.org/10.1051/0004-6361/201424772, https://arxiv.org/abs/arXiv:1502.04957 [astro-ph.SR]

Drechsel H, Lorenz R (1993) Period of SV Centauri Continues Decreasing. Information Bulletin on Variable Stars 3868:1

Drechsel H, Rahe J, Wargau W, et al (1982) The interacting early-type contact binary SV Cen.

A&A110:246–262

Eldridge JJ, Fraser M, Smartt SJ, et al (2013) The death of massive stars - II. Observational constraints on the progenitors of Type Ibc supernovae. Monthly Notices of the Royal Astronomical Society 436:774–795. https://doi.org/10.1093/mnras/stt1612

Fox GK (1991) Stellar Occultation of Polarized Light from Circumstellar Electrons. III. General Axisymmetric Envelopes. ApJ379:663. https://doi.org/10.1086/170540

Fox GK (1994) The Theoretical Polarization of Pure Scattering Axisymmetric Circumstellar Envelopes. ApJ435:372. https://doi.org/10.1086/174819

Giuricin G, Mardirossian F (1981) Some aspects of mass loss and mass transfer in Algol variables. ApJS46:1–26. https://doi.org/10.1086/190732

Giuricin G, Mardirossian F, Mezzetti M (1983) General properties of Algol binaries. ApJS52:35–60. https://doi.org/10.1086/190858

Harmanec P, Morand F, Bonneau D, et al (1996) Jet-like structures in β Lyrae. Results of optical interferometry, spectroscopy and photometry. A&A312:879–896

Hoffman JL, Nordsieck KH, Fox GK (1998) Spectropolarimetric Evidence for a Bipolar Flow in beta Lyrae. AJ115(4):1576–1591. https://doi.org/10.1086/300274

Hoffman JL, Whitney BA, Nordsieck KH (2003) The Effect of Multiple Scattering on the Polarization from Binary Star Envelopes. I. Self- and Externally Illuminated Disks. ApJ598(1):572–587. https://doi.org/10.1086/378770, https://arxiv.org/abs/arXiv:astro-ph/0307261 [astro-ph]

Ignace R, Oskinova LM, Waldron WL, et al (2008) Phase-dependent X-ray observations of the β Lyrae system. No eclipse in the soft band. A&A477(3):L37–L40. https://doi.org/10.1051/0004-6361:20078871, https://arxiv.org/abs/arXiv:0711.3954 [astro-ph]

Ignace R, Fullard A, Shrestha M, et al (2022) Modeling the Optical to Ultraviolet Polarimetric Variability from Thomson Scattering in Colliding-wind Binaries. ApJ933(1):5. https://doi.org/10.3847/1538-4357/ac6fce, https://arxiv.org/abs/arXiv:2205.07612 [astro-ph.SR]

Ivanova N, Justham S, Chen X, et al (2013) Common envelope evolution: where we stand and how we can move forward. A&ARv21:59. https://doi.org/10.1007/s00159-013-0059-2, https://arxiv.org/abs/arXiv:1209.4302 [astro-ph.HE]

Jones CE, Labadie-Bartz J, Cotton DV, et al (2022) Ultraviolet Spectropolarimetry: on the origin of rapidly rotating B stars. Ap&SS 367:**Topical Collection**

Kondo Y, McCluskey GE, Silvis JMS, et al (1994) Ultraviolet Light Curves of beta Lyrae: Comparison of OAO A-2, IUE, and Voyager Observations. ApJ421:787. https://doi.org/10.1086/173691

Kriz S, Harmanec P (1975) A Hypothesis of the Binary Origin of Be Stars. Bulletin of the Astronomical Institutes of Czechoslovakia 26:65

Langer N (2012) Presupernova Evolution of Massive Single and Binary Stars. ARA&A50:107–164. https://doi.org/10.1146/annurev-astro-081811-125534, https://arxiv.org/abs/arXiv:1206.5443 [astro-ph.SR]

Laplace E, Justham S, Renzo M, et al (2021) Different to the core: the pre-supernova structures of massive single and binary-stripped stars. arXiv e-prints arXiv:2102.05036. https://arxiv.org/abs/arXiv:2102.05036 [astro-ph.SR]

Linnell AP, Scheick X (1991) Does SV Centauri Harbor an Accretion Disk? ApJ379:721. https://doi.org/10.1086/170547

Linnell AP, Peters GJ, Polidan RS (1988) An Improved Photometric Analysis of SX Aurigae. ApJ327:265. https://doi.org/10.1086/166187

Lomax JR, Hoffman JL, Elias INicholas M., et al (2012a) Geometrical Constraints on the Hot Spot in Beta Lyrae. ApJ750(1):59. https://doi.org/10.1088/0004-637X/750/1/59, https://arxiv.org/abs/arXiv:1108.3015 [astro-ph.SR]

Lomax JR, Hoffman JL, Elias INicholas M., et al (2012b) Geometrical Constraints on the Hot Spot in Beta Lyrae. ApJ750(1):59. https://doi.org/10.1088/0004-637X/750/1/59, https://arxiv.org/abs/arXiv:1108.3015 [astro-ph.SR]

Lomax JR, Nazé Y, Hoffman JL, et al (2015) V444 Cygni X-ray and polarimetric variability: Radiative and Coriolis forces shape the wind collision region. A&A573:A43. https://doi.org/10.1051/0004-6361/201424468, https://arxiv.org/abs/arXiv:1410.6117 [astro-ph.SR]

Lomax JR, Fullard AG, Malatesta MA, et al (2017) The complex circumstellar and circumbinary environment of V356 Sgr. MNRAS464(2):1936–1947. https://doi.org/10.1093/mnras/stw2457, https://arxiv.org/abs/arXiv:1609.07489 [astro-ph.SR]

Lubow SH, Shu FH (1975) Gas dynamics of semidetached binaries. ApJ198:383–405. https://doi.org/10.1086/153614

Lubow SH, Shu FH (1976) Gas dynamics of semidetached binaries. II. The vertical structure of the stream. ApJ207:L53–L55. https://doi.org/10.1086/182177

Manset N, Bastien P (2000) Polarimetric Variations of Binary Stars. I. Numerical Simulations for Circular and Eccentric Binaries in Thomson Scattering Envelopes. AJ120(1):413–429. https://doi.org/10.1086/301439

Nelson CA, Eggleton PP (2001) A Complete Survey of Case A Binary Evolution with Comparison to Observed Algol-type Systems. ApJ552(2):664–678. https://doi.org/10.1086/320560, https://arxiv.org/abs/arXiv:astro-ph/0009258 [astro-ph]

Nordsieck KH, Wisniewski J, Babler BL, et al (2001) Ultraviolet and visible spectropolarimetric variability in P Cygni. In: de Groot M, Sterken C (eds) P Cygni 2000: 400 Years of Progress, p 261, astro-ph/0102073

Paczyński B (1971) Evolutionary Processes in Close Binary Systems. ARA&A9:183. https://doi.org/10.1146/annurev.aa.09.090171.001151

Peters GJ (1989) The Hα Emitting Regions of the Accretion Disks in ALGOLS. Space Sci. Rev.50(1-2):9–22. https://doi.org/10.1007/BF00215915

Peters GJ (2001) The Algol-Type Binaries. In: Vanbeveren D (ed) The Influence of Binaries on Stellar Population Studies, p 79, https://doi.org/10.1007/978-94-015-9723-4_6

Peters GJ (2007) Bipolar Jets, Hot Interaction Regions, and Colliding Winds in OB Interacting Binaries. In: Hartkopf WI, Harmanec P, Guinan EF (eds) Binary Stars as Critical Tools & Tests in Contemporary Astrophysics, pp 148–153, https://doi.org/10.1017/S174392130700395X

Peters GJ, Polidan RS (1984) Evidence for a high-temperature accretion region in Algol-type binarysystems. ApJ283:745–759. https://doi.org/10.1086/162359

Peters GJ, Polidan RS (2004) Eclipse mapping of the hot circumstellar plasma in Algol binaries. Astronomische Nachrichten 325(3):225–228. https://doi.org/10.1002/asna.200310224

Plavec M (1970) Mass Exchange in Binary Stars. PASP82(489):957. https://doi.org/10.1086/128996

Plavec M (1976) Final Remarks on the Binary Hypothesis for the be Stars. In: Slettebak A (ed) Be and Shell Stars, p 439

Plavec M, Polidan RS (1976) The ALGOLS, Red Spectra, BE Stars, and Even Neutrinos. In: Eggleton P, Mitton S, Whelan J (eds) Structure and Evolution of Close Binary Systems, p 289

Plavec MJ (1980) IUE observations of long period eclipsing binaries: A study of accretion onto

non-degenerate stars. In: Plavec MJ, Popper DM, Ulrich RK (eds) Close Binary Stars: Observations and Interpretation, pp 251–261

Plavec MJ (1983) Far-ultraviolet emission lines in U Cephei : evidence for a hot, turbulent circumstellar envelope. ApJ275:251–270. https://doi.org/10.1086/161530

Sana H, de Mink SE, de Koter A, et al (2012) Binary Interaction Dominates the Evolution of Massive Stars. Science 337:444. https://doi.org/10.1126/science.1223344

Sana H, de Koter A, de Mink SE, et al (2013) The VLT-FLAMES Tarantula Survey. VIII. Multiplicity properties of the O-type star population. Astronomy & Astrophysics, Volume 550, idA107, <NUMPAGES>22</NUMPAGES> pp 550:A107. https://doi.org/10.1051/0004-6361/201219621

Scowen P, Gayley K, Ignace R, et al (2022) The Polstar High Resolution Spectropolarimetry MIDEX Mission. Ap&SS 367:**Topical Collection**

Shrestha M, Neilson HR, Hoffman JL, et al (2018) Polarization simulations of stellar wind bow-shock nebulae - I. The case of electron scattering. MNRAS477(1):1365–1382. https://doi.org/10.1093/mnras/sty724, https://arxiv.org/abs/arXiv:1712.04958 [astro-ph.SR]

Simmons JFL (1982) Analytic treatment of polarization by arbitrary scattering mechanisms in circumstellar envelopes. I - Single stars. MNRAS200:91–113. https://doi.org/10.1093/mnras/200.1.91

Simmons JFL (1983) Analytic treatment of polarization by arbitrary scattering mechanisms in circumstellar envelopes. II - Binary stars. MNRAS205:153–170. https://doi.org/10.1093/mnras/205.1.153

St-Louis N, Gayley KG, Hillier DJ, et al (2022) UV Spectropolarimetry with Polstar: Massive Star Binary Colliding Winds. Ap&SS 9999:**Topical Collection**

Sudar D, Harmanec P, Lehmann H, et al (2011) UX Monocerotis as a W Serpentis binary. A&A528:A146. https://doi.org/10.1051/0004-6361/201014920, https://arxiv.org/abs/arXiv:1103.1766 [astro-ph.SR]

Tauris TM, Kramer M, Freire PCC, et al (2017) Formation of Double Neutron Star Systems. The Astrophysical Journal 846:170. https://doi.org/10.3847/1538-4357/aa7e89

Taylor M, Code AD, Nordsieck KH, et al (1991) First Ultraviolet Spectropolarimetry of Hot Supergiants. ApJ382:L85. https://doi.org/10.1086/186218

van Rensbergen W, De Greve JP, De Loore C, et al (2008) Spin-up and hot spots can drive mass out of a binary. A&A487(3):1129–1138. https://doi.org/10.1051/0004-6361:200809943, https://arxiv.org/abs/arXiv:0804.1215 [astro-ph]

van Rensbergen W, De Greve JP, Mennekens N, et al (2010) Mass loss out of close binaries. Case A Roche lobe overflow. A&A510:A13. https://doi.org/10.1051/0004-6361/200913272, https://arxiv.org/abs/arXiv:0908.2021 [astro-ph.SR]

Wang L, Gies DR, Peters GJ, et al (2021) The Detection and Characterization of Be+sdO Binaries from HST/STIS FUV Spectroscopy. AJ161(5):248. https://doi.org/10.3847/1538-3881/abf144, https://arxiv.org/abs/arXiv:2103.13642 [astro-ph.SR]

Whitney BA, Wood K, Bjorkman JE, et al (2017) HO-CHUNK: Radiation Transfer code. 1711.013

Wood K, Bjorkman JE, Whitney BA, et al (1996) The Effect of Multiple Scattering on the Polarization from Axisymmetric Circumstellar Envelopes. I. Pure Thomson Scattering Envelopes. ApJ461:828. https://doi.org/10.1086/177105

Yoon SC (2015) Evolutionary Models for Type Ib/c Supernova Progenitors. Publ Astron Soc Aust 32:e015. https://doi.org/10.1017/pasa.2015.16, https://arxiv.org/abs/arXiv:1504.01205

Zhao M, Gies D, Monnier JD, et al (2008) First Resolved Images of the Eclipsing and Interacting Binary β Lyrae. ApJ684(2):L95. https://doi.org/10.1086/592146, https://arxiv.org/abs/arXiv:0808.0932 [astro-ph]

Statements & Declarations

This research has made use of NASA's Astrophysics Data System and the SIMBAD database, operated at CDS, Strasbourg, France. The work has also made use of the BeSS database, operated at LESIA, Observatoire de Meudon, France: http://basebe.obspm.fr. This research made use of Astropy, http://www.astropy.org a community-developed core Python package for Astronomy (Astropy Collaboration et al, 2013, 2018).

Funding

GJP gratefully acknowledges support from NASA grant 80NSSC18K0919 and STScI grants HST-GO-15659.002 and HST-GO-15869.001. RI acknowledges funding support from a grant by the National Science Foundation (NSF), AST-2009412. JLH acknowledges support from NSF under award AST-1816944 and from the University of Denver via a 2021 PROF award. YN acknowledges support from the Fonds National de la Recherche Scientifique (Belgium), the European Space Agency (ESA) and the Belgian Federal Science Policy Office (BELSPO) in the framework of the PRODEX Programme (contracts linked to XMM-Newton and Gaia). Scowen acknowledges his financial support by the NASA Goddard Space Flight Center to formulate the mission proposal for *Polstar*.

Competing Interests

The authors have no relevant financial or non-financial interests to disclose.

Author Contributions

All authors shared ideas that motivated this work. We showed how FUV/NUV spectroscopy and spectropolarimetry is key to understanding the evolution of OB close binaries, especially systemic mass and angular momentum loss and transfer. All authors contributed to the writing of the paper. KGG computed the evolutionary tracks in the r-q diagram presented in Section 2 and shown in Figure 1. GJP and KGG were the main contributors to Sections 2 and 3. RI and JLH contributed the calculations and text for Section 4. GJP wrote section 5.

Data Availability

Data sharing is not applicable to this article as no datasets were generated or analysed during the current study.

Affiliations

[1]Department of Physics & Astronomy, University of Southern California, Los Angeles, CA 90089-0484, USA

[2]Department of Physics & Astronomy, University of Iowa, Iowa City, IA, 52242, USA

[3]Department of Physics & Astronomy, East Tennessee State University, Johnson City, TN 37614, USA

[4]Department of Physics and Astronomy, Western University, London, ON N6A 3K7, Canada

[5]GAPHE, University of Liège, Allée du 6 Aout 19c (B5C), 4000-Liège, Belgium

[6]Département de physique, Université de Montréal, Campus MIL, 1375 Avenue Thérèse-Lavoie-Roux Montréal (Qc) H2V 0B3

[7]Department of Physics & Astronomy, University of Auckland, 38 Princes Street, 1010, Auckland, New Zealand

[8]Armagh Observatory and Planetarium, College Hill, BT61 9DG Armagh, Northern Ireland

[9]Department of Physics and Astronomy, Embry-Riddle Aeronautical University, 3700 Willow Creek Rd, Prescott, AZ, 86301, USA

[10]Department of Physics and Astronomy, 2112 E. Wesley Ave., Denver, CO 80208, USA

[11]Physics Department, United States Naval Academy, 572C Holloway Rd, Annapolis, MD 21402, USA

[12]Anton Pannekoek Institute for Astronomy and Astrophysics, University of Amsterdam, 1090 GE Amsterdam, The Netherlands

[13]Department of Physics & Astronomy, Michigan State University,567 Wilson Rd., East Lansing, MI 48824, MI

[14]NASA Goddard Space Flight Center, Greenbelt, MD 20771, USA